1

A change in the relation between the Subtropical Indian Ocean Dipole and the

South Atlantic Ocean Dipole indices in the past four decades

4

Lejiang Yu[1*], Shiyuan Zhong[2], Timo Vihma[3], Cuijuan Sui[4], and Bo Sun[1]

1 MNR Key Laboratory for Polar Science, Polar Research Institute of China,

Shanghai, China,

2 Department of Geography, Environment and Spatial Sciences, Michigan State

University, East Lansing, MI, USA,

3 Finnish Meteorological Institute, Helsinki, Finland

4 National Marine Environmental Forecasting Center, Beijing, China

*Corresponding Author's address Dr. Lejiang Yu

MNR Key Laboratory for Polar Science, Polar Research Institute of China, Shanghai,

China

Jinqiao Road 451, 200136, Shanghai, China

Phone: 0086-020-58712034, email: yulejiang@sina.com.cn

17

18

19

20

21

22

Atmospheric
Chemistry
and Physics

Open Access

EGU

Discussions

23 **Abstract**

24   We utilized the global atmospheric reanalysis (ERA5) and reconstructed sea

25 surface temperature (SST) data from 1979 through 2020 to examine the stability of

26 the relationship between the SST oscillations in the southern Indian and the Atlantic

27 Oceans described by the Subtropical Indian Ocean Dipole (SIOD) and the South

28 Atlantic Ocean Dipole (SAOD) indices. We note a significant positive correlation

29 between the two indices prior to the year 2000 but practically no correlation

30 afterwards. We show that in the two decades prior to 2000, a positive phase of SAOD

31 is associated with more convective activities over the subtropical southern Atlantic

32 Ocean and eastern Brazil, which trigger a stronger upper-atmosphere wavetrain, and

33 further produces stronger southern subtropical highs and surface anti-cyclonic

34 circulations and therefore a stronger correlation between the two indices. The

35 situation is reversed after 2000. Our results are potentially applicable for predictions

36 of precipitation in southern Africa and South America.

37 **1   Introduction**

38   A southwest-northeast-oriented dipole mode characterizes the anomalous sea

39 surface temperature (SST) patterns over the subtropical South Indian and Atlantic

40 Oceans (Wang, 2010). The former is referred to as the Subtropical Indian Ocean

41 Dipole (SIOD) mode (Behera and Yamagata, 2001) and the latter is named as the

42 South Atlantic Ocean Dipole (SAOD) mode (Venegas et al., 1997). The two

43 subtropical modes display similar seasonal variability with their peaks in austral

44 summer (Morioka et al., 2012). Surface latent heat flux anomalies play a vital role in

45   their variability (Sterl and Hazeleger, 2003; Suzukietal., 2004; Hermes and Reason,

46   2005).Moreover, the interannual variability of the two modes has been linked to the El

47   Niño–Southern Oscillation (ENSO) (Boschat et al., 2013). The two subtropical modes

48   exert a great influence on precipitation in Africa and South America (Reason, 2001;

49   2002; Vigaud et al., 2009; Nnamchi and Li, 2011; Morioka et al., 2012; Wainer et al.,

50   2020) and, therefore, understanding the relationship between the two modes has

51   practical implications for precipitation forecasts in Africa and South America on

52   seasonal scale and beyond.

53   Using observational data, Fauchereau et al. (2003) noted the co-variability of the

54   SIOD and SAOD indices in austral summer. Hermes and Reason (2005) confirmed

55   the co-variability of the two indices and attributed it to an anomalous subtropical high.

56   Both studies suggested a linkage between the two indices and an atmospheric zonal

57   wavenumber-4 pattern in the Southern Hemisphere. Lin (2019) also suggested the

58   atmospheric zonal wavenumber-4 pattern controlling the South Atlantic-South Indian

59   Ocean SST pattern. The atmospheric wavenumber-4 was also observed in other

60   studies (Chiswell, 2021; Senapati, et al., 2021). The global wave number-4 pattern in

61   SST includes southern subtropical Indian and Atlantic Ocean components that

62   resemble the two subtropical dipole modes (Senapati et al., 2021). The linkage

63   between the SST patterns in the Southern Hemisphere ocean basins and their relation

64   with atmospheric wavenumber-4 pattern is a challenging and active research topic

65   worthy of further investigation.

66   Although previous studies have suggested that a relationship exists between the

67   SIOD and the SAOD indices, few have focused on the stability of the relationship. In

68   this study, we examine the SIOD-SAOD relationship over the past four decades from

69   1979 through 2020. We underscore a change in the relationship that occurred around

70   2000 and provide a physical explanation for the change.

71   **2   Datasets and methods**

72   Monthly SST data from the United States National Oceanic and Atmospheric

73   Administration (NOAA) Extended Reconstucted SST V5 (Huang et al., 2017) are

74   utilized to calculate the SIOD and SAOD indices. To confirm the results, we also use

75   the Kaplan Extended SST V2 data set from the UK Met Office (Kaplanet al., 1998).

76   Following previous studies, we derive the SOD indexas the difference in the SST

77   anomalies between the western (55-65ºE, 37-27ºS) and eastern (90-100ºE, 28-18ºS)

78   subtropical Indian Ocean(Behera and Yamagata, 2001) and the SAOD index as the

79   difference of SST anomalies between the south-western (10-30ºW, 30-40ºS) and

80   north-eastern (0-20ºW, 15-25ºS) South Atlantic Ocean (Morioka et al., 2011).

81   Atmospheric data from the European Centre for Medium-Range Weather Forecasts

82   (ECMWF) fifth-generation reanalysis (ERA5, Hersbach et al., 2020) provide 200-hPa

83   and surface atmospheric variables. We also employ monthly top-of-atmosphere (TOA)

84   outgoing longwave radiation (OLR) from the NOAA Interpolated OLR dataset

85   (Liebmann and Smith, 1996).

86   Correlation and regression analyses are utilized to examine the relationship

87   between the SIOD and the SAOD indices. The confidence levels are determined by

88   the two-tailed Student's t test. Before the correlation or regression analyses are

89 applied to the data, the variables and indices are detrended. We also remove the

90 influence from the ENSO signal using the method proposed by An (2003), where the

91 ENSO signal is represented by the Niño 3.4 index. The generation and propagation of

92 planetary waves are identified on the basis of the Rossby wave source (RWS) and the

93 wave activity flux (WAF). The RWS is calculated following Sardeshmukh and

94 Hoskins (1988) and the WAF is derived using the method of Takaya and Nakamura

95 (2001). Notice that due to the peak of the SIOD and SAOD in February (Morioka et

96 al., 2012), the austral seasons in this study refer to summer (January-March), autumn

97 (April-June), winter (July-September), and spring (October-December).

98 **3 Results**

99 The spatial patterns of temporal anomalies of SST depicted by SIOD and SAOD

100 indices display southwest-northeast-oriented dipoles in the subtropical southern

101 Indian Ocean (SIOD, Figure 1a) and Atlantic Ocean (SAOD, Figure 1b).Using the

102 NOAA Extended Reconstucted SST V5 data, the correlations between the SIOD and

103 SAOD indices over the 42-year period are 0.56 for austral summer ($p<0.05$),

104 becoming insignificant in other seasons with correlation coefficients dropping by

105 nearly half to 0.23 for austral autumn and winter and 0.25 for austral spring.

106 Removing the ENSO signal resulted in small changes in the correlations and their

107 seasonal variations, with summer being the only season when the two indices are

108 significantly correlated (0.45, $p<0.01$) (Figure 1c). The Kaplan Extended SST V2 data

109 yielded similar results, with slightly lower summertime correlation coefficients: 0.49

110 (with ENSO signal) and 0.38 (without ENSO signal, $p<0.05$). Henceforth, we focus

111   on the summer time series without the ENSO signal.

112   To assess the stability of the SIOD-SAOD correlation over the past four decades,

113   we calculate moving correlation of the two indices using 15-year and 20-year sliding

114   windows (Figure 1d). For the 15-year window, the correlation is above (below) the 95%

115   confidence level before (after) 1998 and for the 20-year sliding window the shifting

116   occurs in 2003. Similar results are obtained using the Kaplan Extended SST V2 data

117   (Figure 2). There is a remarkable difference in the correlation between the two indices

118   prior to and after 1999 (Figure 1d). For the 1979-1999 period, the correlation

119   coefficient is 0.64($p<0.01$), dropping sharply to only 0.19 ($p>0.05$) for the 2000-2020

120   period. Results derived using the Kaplan Extended SST V2 data are almost similar,

121   with the correlation coefficients of 0.60 ($p<0.01$) for the 1979-1999 period and 0.20

122   ($p>0.05$) for the 2000-2020 period. This notable drop in the correlation between the

123   SIOD and SAOD indices from the first two decades to the next two warrants further

124   investigation. Below we explore the reasons behind the change.

125   We compare the regression maps of the Southern Hemisphere SST anomalies onto

126   the summertime SAOD and SIOD indices for the 1979-1999 period with those for the

127   2000-2020 period (Figure 3). There are clear differences in the anomalous SST

128   patterns between the two periods. As a response to the positive phase of the SAOD

129   index, significant SST anomalies occur in the southern subtropical Indian Ocean

130   during the 1979-1999 period, with a spatial pattern(Figure 3a) closely resembling the

131   positive phase SIOD index (Figure 1a); however, the SST anomalies for the

132   2000-2020 period are not significant in the southern subtropical Indian Ocean(Figure

133   3b). Similarly, corresponding to the SIOD index, a dipole of significant SST

134   anomalies appears in the South Atlantic Ocean (Figure 3c) for the 1979-1999 period

135   that bear strong resemblance to the positive phase SAOD pattern (Figure 1b), whereas

136   for the 2000-2020 period, the SST anomalies are insignificant (Figure 3d). These

137   results confirm the strong correlation between the SAOD and SIOD indices during the

138   first two decades and the lack of correlation in last two decades, separated by the turn

139   of the century.

140   Lin (2019) relateda South Atlantic-South Indian Ocean pattern to a wavetrain

141   induced by the South Atlantic Convergence Zone anomaly. We hypothesize that the

142   stability of the SAOD-SIOD relation may also be related to the strength of the

143   wavetrain. To test this hypothesis, we examine the regression patterns of several

144   atmospheric variables related to convective and wave activities (OLR, RWS, WAF,

145   200-hPa divergent wind, and streamfunction), to the SAOD index in austral summer

146   separately for the 1979-1999 period and the 2000-2020 period (Figure 4). Over the

147   1979-1999 period, corresponding to the positive phase of the SAOD index,

148   convective activities are enhanced over the southern subtropical Atlantic Ocean and

149   eastern Brazil, which are flanked by suppressed convective activities over tropical and

150   mid-latitude South Atlantic Ocean (Figure 4a). The convective activities over western

151   subtropical southern Atlantic Ocean and eastern Brazil produce positive RWS and

152   200-hPa divergent wind (Figure 4c),which trigger a wavetrain propagating

153   southeastwards into the South Atlantic Ocean, and then eastwards into the South

154   Indian Ocean, Australia and the South Pacific Ocean (Figure 4e). The wavetrain

155   generates negative streamfunction anomalies over the South Indian and Atlantic

156   Oceans (Figure 4e). In contrast, over the 2000-2020 period, the magnitude of the

157   anomalous OLR is less significant than that over the 1979-1999 period (Figure 4b).

158   Weaker RWS and upper level divergent wind (Figure 4d) indicate a weaker wavetrain,

159   which results in weaker streamfunction anomalies over the South Atlantic and Indian

160   Oceans (Figure 4f).

161   Although the magnitudes of the SST anomalies related to the SAOD index are

162   comparable over the two periods (Figure 4a and 4b), the anomalous OLR and RWS

163   and the related wavetrain associated with the SAOD index are substantially different

164   between the two periods. The differences in the climatological conditions over the two

165   periods may provide a plausible explanation. For example, over the subtropical

166   southern Atlantic Ocean and most of Brazil, OLR anomalies are generally negative

167   during the 1979-1999 period, suggesting stronger convective activity favorable for the

168   generation of the wavetrain (Figure 5a), but in contrast, OLR anomalies are mostly

169   positive during 2000-2020, indicating suppressed convective activities unfavorable

170   for the formation of the wavetrain (Figure 5b). Thus, the interdecadal variability of

171   the OLR activities can modulate the effect of the SAOD mode on atmospheric

172   circulation patterns over other ocean basins.

173   Similarly, we have also obtained the patterns of the aforementioned atmospheric

174   circulation variables associated with the SIOD index separately for the two periods

175   (Figure 6). During 1979-1999, the anomalous OLR, RWS and 200-hPa divergent

176   wind fields favor the causal chain for the wavetrain generation, but this is not the case

177 during 2000-2020.

178   The SAOD and SIOD modes are related to the subtropical highs in the South

179 Atlantic and Indian Oceans, with stronger high corresponding to the positive phase of

180 the two indices due to wind-induced evaporation (Wang, 2010; Behera and Yamagata,

181 2001; Venegas et al., 1997). We proceed to examine the climatological mean sea level

182 pressure and surface wind field related to the aforementioned wavetrain over the two

183 periods (Figure 7). The position and strength of the climatological subtropical highs

184 and the associated surface winds in the southern Indian and the Atlantic Oceans show

185 little difference over the two periods (Figure 7a and 7b). However, the regression of

186 the mean sea level pressure to the SAOD index for the two periods show considerably

187 stronger subtropical highs and anti-cyclonic circulations in the South Atlantic and the

188 Indian Oceans over the 1979-1999 period than the 2000-2020 period (Figure 7c and

189 7d). According to the study of Hermes and Reason (2005), a stronger subtropical high

190 favors larger magnitude of the SST anomalies represented by the SAOD and SIOD

191 indices. The large decrease in the strength of the summertime subtropical high

192 associated with SAOD from the first two decades to the next two (Figure 7c, 7d)

193 corroborates the sharp drop in the SAOD-SIOD correlation (Figure 1d).

194 **4   Conclusion and discussion**

195   In this study, we examined the relation between the oscillations of the SST in the

196 subtropical South Indian and the Atlantic Oceans described by the SIOD and SAOD

197 indices and the stability of the relation using the ERA5 global atmospheric reanalysis

198 and reconstructed SST data from 1979 through 2020. We found significant relation

199   between the two indices in austral summer. Through moving correlation analyses, we

200   discovered that the relation in austral summer was not stable for the past four decades.

201   Specifically, the correlation between the two indices was significant prior to 2000 but

202   insignificant afterwards. The change in the relation between the two indices is

203   attributed to a change in the strength of the atmospheric wavetrain induced by

204   anomalous convective activity over the subtropical southern Atlantic Ocean and

205   eastern Brazil. More convective activities prior to 2000 excited stronger wavetrain,

206   which produced stronger subtropical highs during the positive phase of SAOD,

207   resulting in a stronger relation between the two indices. The opposite occurred after

208   2000.

209   The interdecadal variability of OLR over the subtropical South America and

210   Atlantic Ocean is key to the relation between the SAOD and SIOD indices. What

211   determined the OLR anomalies in the region prior to and after 2000 needs to be

212   further investigated. Hermes and Reason (2005) suggested that the southern

213   subtropical high is related to the Antarctic Oscillation (AAO) and the linkage

214   strengthened after mid-1970s. The influence of the change in the AAO index on the

215   relation between the SAOD and the SIOD indices needs to be assessed. Yu et al.

216   (2017) noted a phase change of the Atlantic Multidecadal Oscillation (AMO) and the

217   Pacific Decadal Oscillation (PDO) indices in the late 1990s, with PDO shifting from

218   positive to negative and AMO switching from negative to positive around 1999. Dong

219   and Dai (2015) noted the influence of IPO on precipitation in Brazil. However, the

220   influence from the same phase of the IPO has great uncertainty and depends on the

Atmospheric
Chemistry
and Physics

Discussions

Open Access

EGU

221   period and dataset (Dong and Dai, 2015). Jones and Carvalho (2018) suggested more

222   precipitation in Brazil during the negative phase of the AMO than during its positive

223   phase. Longer datasets are utilized to examine the effect of the IPO and AMO on

224   convective activity over the subtropical South America and Atlantic Oceanon the

225   interdecadal time scale. Although our results are only based on statistical analyses,

226   they have potential for improving the prediction of precipitation in southern Africa

227   and South America.

228   *Data Availability*

229   The monthly SST data from the U.S. NOAA Extended Reconstructed Sea Surface

230   Temperature (ERSST) version 5 (ERSST v5) are available online

231   (https://www1.ncdc.noaa.gov/pub/data/cmb/ersst/v5/netcdf/).Kaplan Extended SST

232   V2 data are derived from below website

233   (https://psl.noaa.gov/cgi-bin/db_search/DBSearch.pl?Dataset=Kaplan+Extended+SST

234   +V2&Variable=Sea+Surface+Temperature).The monthly ERA5 reanalysis data are

235   available from the Copernicus Climate Data Store

236   (https://www.ecmwf.int/en/forecasts/datasets/reanalysis-datasets/era5). The monthly

237   OLR data are derived from the NOAA Interpolated OLR

238   (https://psl.noaa.gov/cgi-bin/db_search/DBSearch.pl?Dataset=NOAA+Interpolated+O

239   LR&Variable=Outgoing+Longwave+Radiation).

240   *Acknowledgments*

Atmospheric
Chemistry
and Physics

Discussions

246   *Author contributions*. LY designed the research, analyzed the data, and wrote the first

247   draft of the paper. S Z and TV revised the first draft and provided useful insights

248   during various stages of the work. CS and BS provided some comments and helped

249   with editing the paper.

250   *Competing interests*. The authors declare that they have no conflict of interest.

251   **References**

252   An, S. I.: Conditional maximum covariance analysis and its application to the

253   tropical Indian Ocean SST and surface wind stress anomalies, J. Climate, 16,

254   2932–2938, 2003.

255   Behera, S. K., and Yamagata, T.: Subtropical SST dipole events in the southern

256   Indian Ocean, Geophys. Res. Lett., 28, 327-331, 2001.

257   Boschat, G, Terray, P., and Masson, S.: Extratropical forcing of ENSO, Geophys. Res.

258   Lett., 40, 1605-1611, 2013.

259   Chiswell, S. M.: Atmospheric wavenumber-4 driven South Pacific marine heat waves

260   and marine cool spells, Nature Communication, 12, 4779, 2021.

261   Dong, B., and Dai, A.: (2015).The influence of the Interdecadal Pacific Oscillation on

262   temperature and precipitation over the global, Clim. Dyn., 45, 2667-2681.

263   Fauchereau, N., Trzaska, S., Richard, Y., Roucou, P., and Camberlin, P.: Sea

264   Surface temperature co-variability in the Southern Atlantic and Indian Oceans

265   And its connections with the atmospheric circulation in the Southern

266   Hemisphere, Int. J. Climatol., 23, 663–677, 2003.

267   Hermes, J. C., and Reason, C. J. C.: Ocean model diagnosis of interannual coevoling

268   SST variability in the South Indian and South Atlantic Oceans, J. Climate, 18,

269   2864-2882, 2005.

270   Hersbach, H., Bell, B., Berrisford, P., Hirahara, S., Horányi, A., Muñoz-Sabater, J.,

271   Nicolas, J., Peubey, C., Radu, R., Schepers, D., Simmons, A., Soci, C., Abdalla,

272   S., Abellan, X., Balsamo, G., Bechtold, P., Biavati, G., Bidlot, J., Bonavita, M.,

273   De Chiara, G., Dahlgren, P., Dee, D., Diamantakis, M., Dragani, R., Flemming,

274   J., Forbes, R., Fuentes, M., Geer, A., Haimberger, L., Healy, S., Hogan, J. R.,

275   Hólm, E., Janisková, M., Keeley, S., Laloyaux, P., Lopez, P., Lupu, C., Radnoti,

276   G., de Rosnay, P. Rozum, I., Vamborg, F., Villaume, S., and Thépaut J.-N.: The

277   ERA5 global reanalysis, Quarterly Journal of the Royal Meteorological Society,

278   146, 1999-2049, 2020.

279   Huang, B., Thorne, P. W., Banzon,V. F., and Zhang, H. M.: Extended Reconstructed

280   SeaSurface Temperature version 5 (ERSSTv5), Upgrades, validations, and

281   Intercomparisons, J. Climate, 30, 8179-8205, 2017.

282   Jones, C., and Carvalho, L. M. V.: The influence of the Atlantic multidecadal

283   oscillation on the eastern Andes low-level jet and precipitation in South

284   America, npj Climate and Atmospheric Science, 1, 40, 2018.

285   Kaplan, A., Cane, M., Kushnir, Y., Clement, A., Blumenthal, M., and Rajagopalan, B.:

286   Analyses of global sea surface temperature 1856-1991, J. Geophys. Res., 103,

287   18567-18589, 1998.

288   Liebmann, B., and Simth, C. A.: Description of a complete (interpolated)

289   outgoinglongwave radiation dataset, Bulletin of the American Meteorological

290   Society, 77, 1275–1277, 1996.

291   Morioka, Y., Tozuka, T., and Yamagata, T.: On the growth and decay of the

292   subtropical dipole mode in the south Atlantic. J. Climate, 24, 5538-5554, 2011.

293   Morioka, Y., Tozuka, T., Masson, S., Terray, P., Luo, J.-J., and Yamagata, T.:

294   Subtropical dipole modes simulated in a coupled general circulation mode, J.

295   Climate, 25, 4029-4047, 2012.

296   Nnamchi, H. C., and Li, J. P.: Influence of the South Atlantic Ocean Dipole on West

297   African summer precipitation, J. Climate, 24, 1184-1197, 2011.

298   Reason, C. J. C.: Subtropical Indian Ocean SST dipole events and southern

299   African rainfall, Geophys. Res. Lett., 28, 2225–2227, 2001.

Atmospheric
Chemistry
and Physics
Discussions

300   Reason, C. J. C.: Sensitivity of the southern African circulation to dipole sea-surface

301   temperature patterns in the South Indian Ocean, Int. J. Climatol., 22, 377–393,

302   2002.

303   Sardeshmukh, P. D., and Hoskins, B. J.: The generation of global rotational flow

304   by steady idealized tropical divergence, J. Atmos. Sci., 45, 1228–1251, 1988.

305   Senapati, B., Deb, P., Dash, M. K., and Behera, S. K.: Origin and dynamics of

306   global atmospheric wavenumber-4 in the Southern mid-latitude during austral

307   summer. Climate Dynamics, doi:10.1007/s00382-021-06040-z, 2021.

308   Senapati, B., Dash, M. K., and Behera, S. K.: Global wave number-4 pattern in

309   the southern subtropical sea surface temperature, Scientific Reports, 11, 142,

310   doi:10.1038/s41598-020-80492-x, 2021.

311   Sterl, A., and Hazeleger, W.: Coupled variability and air-sea interaction in the

312   South Atlantic Ocean. Climate Dyn., 21, 559–571, 2003.

313   Suzuki,R.,Behera,S.K., Iizuka,S., and Yamagata, T.: IndianOcean Subtropical dipoles

314   simulated using a coupled general circulation model. J. Geophys. Res., 109,

315   C09001, doi:10.1029/2003JC001974, 2004.

316   Takaya, K., and Nakamura, H.: A formulation of a phase in dependent wave-activity

317   flux for stationary and migratory quasi geostrophic eddies on a zonally varying

318   basic flow. J. Atmos. Sci., 58, 608–627, 2001.

319   Vigaud, N., Richard, Y., Rouault, M., and Fauchereau, N.: Moisture transport between

320   The South Atlantic Ocean and southern Africa: Relationships with summer

321   rainfall and associated dynamics. Climate Dyn., 32, 113–123, 2009.

322   Venegas, S. A., Mysak, L. A., and Straub, D. N.: Atmosphere–ocean coupled

323   variability in the South Atlantic, J. Climate, 10, 2904–2920, 1997.

324   Wainer, I., Prado, L. F., Khodri, M., and Otto-Bliesner, B.: The South Atlantic

325   subtropical dipole mode since the last deglaciation and changes in rainfall,

326   Climate Dynamics, 56,109-122, doi:10.1007/s00382-020-05468-z, 2020.

327   Wang, F.: Subtropical dipole mode in the Southern Hemisphere: A global view.

328   Geophs. Res. Lett., 37, L10702, doi:10.1029/2010GL042750, 2010.

329   Yu, L., Zhong, S., Winkler, J. A., Zhou, M., Lenschow, D. H., Li, B., Wang, X., and

330   Yang, Q.: Possible connection of the opposite trends in Arctic and Antarctic
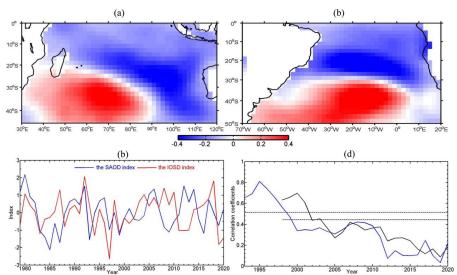
331   sea ice cover. Scientific Reports, 7, 45804, 2017.

332

333

334

335

336

337

338

339

340

341

342

343

344

345

346

Figure 1. Spatial patterns of austral summer (JFM) SST anomalies (°C) for the positive phases of the indices of (a) the Subtropical Indian Ocean Dipole (SIOD)),(b) the South Atlantic Ocean Dipole (SAOD), and (c) their time coefficients), as well as (d) the moving correlations between the detrended and ENSO-signal-removed SIOD and SAOD indices (time coefficients) using the 20-year sliding window (black sold line) and 15-year sliding window (blue solid line). In (d), dashed lines denote the correlation coefficients with the 95% confidence level for 20 samples (black line) and 15 samples (blue line) andthe abscissa indicates the end year of the moving correlations. The above results are derived using the NOAA Extended Reconstucted SST V5 data.
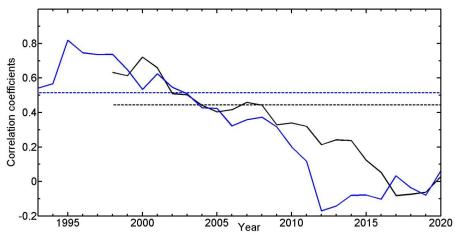
Figure 2 Moving correlations of the IOSD and SAOD indices using the 20-year sliding window (black sold line) and 15-year sliding window (blue solid line) (d). The two indices are removed from the ENSO signal and their trends. Dashed lines denote the correlation coefficients with the 95% confidence level for 20 samples (black line) and 15 samples (blue line). Abscissa indicates the end year of the moving correlations. The above results use Kaplan Extended SST V2 data.
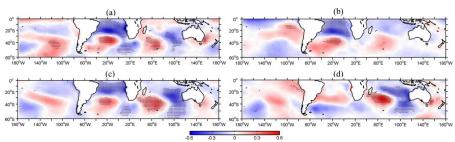
Figure 3.Regression maps of the SST anomalies (°C) onto the summertime indices of (a, b) SAOD and (c, d) SIOD, over the periods of (a, c) 1979-1999 and (b, d) 2000-2020. Dots denote the regions of above 95% confidence level.
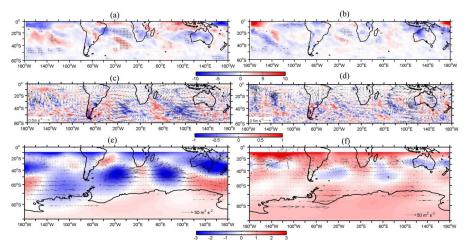
401
402
403
404
405
406
407
408
409
410
411
412
413
414
415
416
417
418
419
420
421
422
423
424
425
426
427
428
429
430
431
432
433
434
435
436
437

438

439

440 Figure 4. Regression maps of (a, b) the outgoing longwave radiation (OLR) (W m^{-2}) at the top of
441 the atmosphere, (c, d) Rossby wave source (RWS) (10^{-10}s^{-2}) and 200-hPa divergent wind (vector),
442 and (e, f) wave activity flux (vector) and streamfunction (m^2 s^{-1}) onto the summertime SAOD
443 index over the periods of (a, c, e) 1979-1999 and (b, d, f) 2000-2020.

444
445
446
447
448
449
450
451
452
453
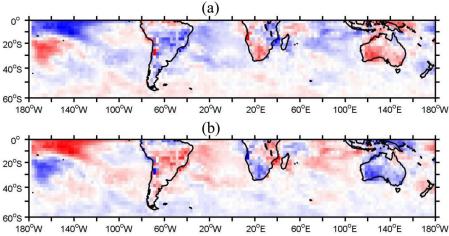454
455
456
457
458
459
460
461
462
463
464
465
466
467
468

Figure 5. Climatological OLR anomalies during (a) 1979-1999 and (b) 2000-2020, with respect to the 42-year climatology over the 1979-2020 period.
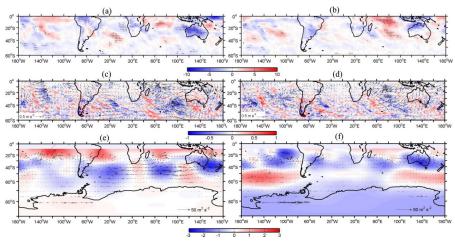
499

Figure 6. Regression maps of outgoing longwave radiation (OLR) (W m^{-2}) (a), (b), Rossby wave
source (RWS) (10^{-10} s^{-2}) and 200-hPa divergent wind (vector) (c), (d), wave activity flux (vector)
and streamfunction (m^2 s^{-1}) (e), (f) onto the summertime IOSD index over the 1979-1999 period
(a), (c), (e) and the 2000-2020 period (b), (d), (f).

504
505
506
507
508
509
510
511
512
513
514
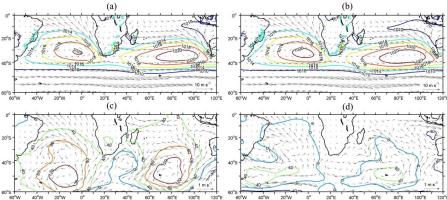515
516
517
518
519
520
521

Figure 7. Climatological mean sea level pressure (MSLP, in hPa) and 10-m wind field (vector) over the periods of (a) 1979-1999 and (b) 2000-2020, and regression maps of MSLP (in Pa) and 10-m wind field (vector)onto the summertime SAOD index over the periods of (c) 1979-1999 and(d) 2000-2020.